A Joint Delay-and-Sum and Fourier Beamforming Method for High Frame Rate Ultrasound Imaging

Wei Zhao[1, 2], Shuai Feng[1], Yadan Wang[1], Yuanguo Wang[1], Zhihui Han[1] and Hu Peng[1, *]

Abstract: Frame rate is an important metric for ultrasound imaging systems, and high frame rates (HFR) benefit moving-target imaging. One common way to obtain HFR imaging is to transmit a plane wave. Delay-and-sum (DAS) beamformer is a conventional beamforming algorithm, which is simple and has been widely implemented in clinical application. Fourier beamforming is an alternative method for HFR imaging and has high levels of imaging efficiency, imaging speed, and good temporal dynamic characteristics. Nevertheless, the resolution and contrast performance of HFR imaging based on DAS or Fourier beamforming are insufficient due to the single plane wave transmission. To address this problem, a joint DAS and Fourier beamforming method is introduced in this study. The proposed method considers the different distributions of sidelobes in DAS imaging and Fourier imaging and combines the angular spectrum and DAS to reconstruct ultrasound images. The proposed method is evaluated on simulation and experimental phantom datasets to compare its performance with DAS and Fourier beamforming methods. Results demonstrate that the proposed method improves image effective dynamic range and resolution while also retaining a high frame rate of the ultrasound imaging systems. The proposed method improves the effective dynamic range along axial and lateral directions by 10 dB, compared to standard DAS and Fourier beamforming.

Keywords: High frame rate imaging, delay-and-sum, Fourier transformation, angular spectrum.

1 Introduction

Ultrasound imaging has been widely implemented for clinical diagnosis and research [Peng and Peng (2012)]. Frame rate is an important metric for ultrasound imaging systems. High frame rates (HFR) will benefit moving-target imaging and reducing the number of transmissions is an effective way to improve frame rate. The frame rate of an imaging system is significantly improved by emitting a plane wave a single time [Han,

[1] Department of Biomedical Engineering, Hefei University of Technology, Hefei, 230009, China.
[2] Yijishan Hospital of Wannan Medical College, Wuhu, 241001, China.
[*] Corresponding Author: Hu Peng. Email: hpeng@hfut.edu.cn.
Received: 09 December 2019; Accepted: 26 December 2019

Peng, Zhao et al. (2018)]. The beamforming algorithm is one of the most vital techniques in HFR imaging systems, determining the imaging quality and effectiveness. The delay-and-sum (DAS) beamformer [Ranganathan and Walker (2003)], as a conventional beamforming method, calculates the propagation time depending on the two-way time-of-flight from the transmit element position to the imaging point position (and back) to the receiving element position. Although the DAS beamformer is simple, its computational load is large and the imaging quality is insufficient. To improve imaging quality, synthetic aperture ultrasound imaging has been studied. This will result in slow imaging speed because multiple transmissions are performed, and also causes insufficient improvement of image quality. Thus, many adaptive weighting techniques have been developed [Synnevag, Austeng and Holm (2007)]. However, these weighting techniques are inherently in the range of the DAS technique [Synnevag, Austeng and Holm (2009); Zhao, Wang, Guo et al. (2016); Diamantis, Greenaway, Anderson et al. (2017); Zheng, Wang, Peng et al. (2020); Wang, Zheng, Peng et al. (2018)] because they are implemented on the delay-compensated data.

The non-diffraction beam [Lu and Greenleaf (1990)], which in theory has a time-invariant wave front along the propagation direction, was widely studied during the 1990s. Lu conducted further research on the non-diffraction beam and proposed a Fourier-based beamforming algorithm for ultrasound imaging [Du, Peng, Jiang et al. (2007); Lu (1997)]. In this method, the array beam is transmitted and the backscattered echo signals are weighted by array beams with different parameters. Then, the image spectrum is obtained through parameter transform, and the reconstructed image is obtained by Fourier transformation. The imaging speed of this method is fast because of the single transmission of a non-diffraction wave, additionally, the Fourier transformation is the main algorithm. Thus, Lu named this method the Fourier method (FM). In our previous study, the non-diffraction beam and FM beamforming were further interpreted using the theory of angular spectrum propagation [Peng, Lu and Han (2006); Wei and Peng (2014)]. We previously proposed to obtain the image spectrum by conducting the Fourier transformation on the echo signals rather than weighting by array beams, further improving the effectiveness of this imaging algorithm.

The imaging quality of the non-diffraction based Fourier beamforming is similar to DAS because it only requires one transmission to form an image [Lu and Cheng (2005)]. To improve image quality, Lu proposed to transmit multiple array beams to obtain an image. This method can effectively extend the imaging spectrum [Cheng and Lu (2006)], and thus reduce noises in the echo signals and improve image quality. However, the imaging speed and the frame rate of imaging system are reduced because the required imaging time becomes longer due to multiple transmissions.

The dynamic characteristics of the HFR imaging system is advantageous because a single transmission improves the imaging frame rate. The imaging frame rate will approach 3700 frames per second when the imaging depth is 200 mm. Thus, it is well suited for the imaging of moving tissue, such as heart. HFR imaging has been a research hotspot in the field of ultrasound imaging [Chen, Hendriks, van Sloun et al. (2018); Chau, Lavarello and Dahl (2016)] with the important goal of improving imaging quality while retaining high frame rates.

2 Theory

In the HFR ultrasound imaging, a plane wave is usually used to be transmitted. An image is obtained by transmitting one plane wave. A commonly used method for data processing is the DAS based HFR (DAS-HFR). Another beamforming technique is the Fourier method based HFR (FM-HFR) which we use the angular spectrum to realize. In this section, DAS-HFR and FM-HFR are first introduced, and then the proposed method is presented.

2.1 DAS-HFR in plane wave field

The DAS beamforming method is a traditional beamformer to reconstruct ultrasound images, which performs delay and sum processes on the echo signals under a known acoustic field. In this study, the plane wave field using all elements for transmitting was used.

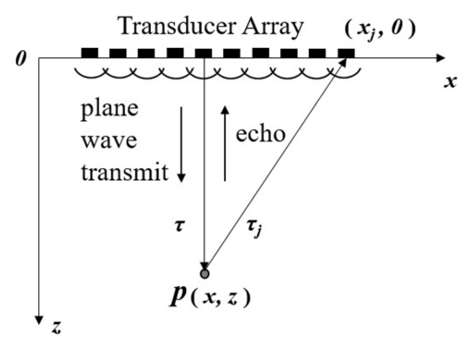

Figure 1: Geometrical model for DAS-HFR imaging system

As shown in Fig. 1, a linear array is excited simultaneously to transmit a plane wave. Assume that $a(t)$ is the excitation signal. For an imaging point $p(x,z)$, the received signal is $a(t-\tau)$, and τ is the time of the pulse wave propagating to the imaging point p. Then the echo signals reflected from point p is received by the j-th element located at $(x_j,0)$, and τ_j is the propagation time of echo signal from point p to the j-th receive element. The DAS output of point p is expressed as

$$f_{DAS}(x,z)=\sum_{j=0}^{N-1} a(t-\tau-\tau_j) \tag{1}$$

Assume c is the speed of sound, and τ and τ_j are calculated as

$$\tau=\frac{z}{c} \tag{2}$$

$$\tau_j=\sqrt{(x-x_j)^2+z^2} \tag{3}$$

2.2 FM-HFR based on angular spectrum

The array beam is emitted by a transducer array, and then reflected by imaging targets during propagating as shown in Fig. 2. The ultrasound transducer is located at the (x, y) plane with $z=0$. The center of the transducer is located at the origin of coordinates. The ultrasound transducer array is switched to receive the echo signals reflected from imaging targets when the emission event is completed. Finally, an ultrasound image can be reconstructed using the recorded echo signals.

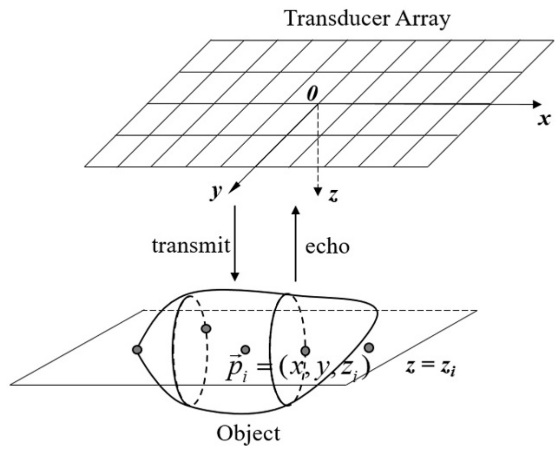

Figure 2: Geometrical model for FM-HFR imaging system

In this study, we select the plane wave, which is a special array beam, as the transmit beam to make it consistent with that of DAS-HFR. The transducer first emits a plane wave, and the acoustic wave signal for the imaging point $\vec{p}_i = (x, y, z_i)$ is $a(t-\tau_i)$ as the pulsatile plane wave reaches $z = z_i$, where $\tau_i = z_i / c$. After Fourier transformation, the spectrum of $a(t-\tau_i)$ is $A(k)e^{jkz_i}$, where $k = w/c$. For scatters in the (x, y) plane at $z = z_i$, the reflected echo signals are

$$s(\vec{p}_i, k) = f(\vec{p}_i)A(k)e^{jkz_i} \tag{4}$$

where $f(\vec{p}_i)$=$f(x, y, z_i)$ is the reflection coefficient function of the scatter. After Fourier transformation, the Eq. (4) in angular spectrum domain (k_x, k_y) is obtained as

$$S_i(k_x, k_y, k, z_i) = \int_{x,y} f(\vec{p}_i)A(k)e^{jkz_i}e^{ik_x x + ik_y y}dxdy \tag{5}$$

Because of the reflection from scatters, the echo signal expressed by the Eq. (5) propagates to the receive transducer. According to the principle of angular spectrum propagation, the received signal is

$$Y_i(k_x, k_y, k; z_i) = S_i(k_x, k_y, k, z_i)e^{i\sqrt{k^2-k_x^2-k_y^2}z} \tag{6}$$

Actually, the echo signal reflects from multiple planes in the acoustic field. Thus, the received signal is actually the sum of the signal from different planes,

$$Y(k_x,k_y,k) = \int_z Y_i(k_x,k_y,k;z_i)dz_i \tag{7}$$

By combining Eqs. (5) and (6), the received signal in Eq. (7) can be expressed as

$$Y(k_x,k_y,k) = \int_{x,y,z} f(\vec{p}_i)A(k)e^{ik_x x + ik_y y + ik_z^{'} z_i} dxdydz_i \tag{8}$$

where

$$k_z^{'} = k + \sqrt{k^2 - k_x^2 - k_y^2} \tag{9}$$

The excited signal spectrum $A(k)$ in Eq. (8) is independent on the integral, and can be introduced from the integral. In this case, the integral is the Fourier transformation of the reflected function $f(x,y,z)$, that is

$$Y(k_x,k_y,k) = A(k)F(k_x,k_y,k_z^{'}) \tag{10}$$

We define

$$F_{FM}(k_x,k_y,k_z^{'}) = Y(k_x,k_y,k) \tag{11}$$

The relationship between $k_z^{'}$ and k is referred to Eq. (9). In consideration of the influence of the signal bandwidth, the measured object can be obtained

$$y_{FM}(x,y,z) = F^{-1}[Y_{FM}(k_x,k_y,k_z^{'})] \tag{12}$$

where $F^{-1}[.]$ is inverse Fourier transformation.

2.3 proposed method

For two-dimensional B-mode ultrasound imaging, the reflection coefficient function $f(x,y,z)$ is a constant in the y direction. Without loss of generality, y can be chosen to 0. Thus, the function $f(x,y,z)$ degenerates to $f(x,z)$, and $F_{FM}(k_x,k_y,k_z^{'})$ degenerates to $Y_{FM}(k_x,k_z^{'})$.

$$y_{FM}(x,z) = F^{-1}[Y_{FM}(k_x,k_z^{'})] \tag{13}$$

The final imaging output can be obtained by combining the output of DAS-HFR,

$$f_{final}(x,z) = f_{DAS}(x,z) \times y_{FM}(x,z) \tag{14}$$

3 Simulation and experiment results

3.1 Data sets description

The aforementioned methods were validated using the data sets provided by the IUS 2016 beamforming challenge held at the 2016 IEEE International ultrasonic forum [Liebgott, Rodriguez-Molares, Cervenansky et al. (2016)]. A set of simulated data and a set of experimental data were selected. The data were in RF format and in the experiment, sampling frequency was 20.832 MHz. Each data set was obtained from 75 guided plane waves covering an angle span of 16 degrees. Here, we only took the echo data of the plane wave propagating along the z-axis.

The transducer parameters used in the simulation and experiment are consistently configured. The transducer is a 128-element linear array with a 0.3 mm pitch, in which an element has a size of 0.27 mm (width) and 5.0 mm (height). The excitation pulse was a sine wave with two half cycles. The center frequency was 5.208 MHz, and the spectrum width was 67% of the center frequency. The transmitting ultrasound field and echo data were calculated by the filed II [Jensen and Svendsen (1992); Jensen (1996)] simulation software.

3.2 Simulation result

The simulation phantom consisted of 20 scattering points, which formed a structure of two horizontal lines and one vertical line.

Fig. 3 shows the imaging results of scattering point targets. The display dynamic range was set as 60 dB. It can be seen that the imaging quality of both FM-HFR algorithm (Fig. 3(a)) and DAS-HFR algorithm (Fig. 3(b)) is poor, and both imaging resolution and contrast are relatively low. Additionally, further observation reveals that the sidelobe distributions of the two imaging results are different. The sidelobe distribution of FM-HFR imaging in Fig. 3(a) is mainly along the horizontal and vertical directions, while the sidelobe distribution of DAS-HFR imaging in Fig. 3(b) is at another angle. This suggests that if we use the DAS-HFR result to weight the FM-HFR result, the sidelobe of the image can be reduced to some extent and the imaging resolution and contrast will be effectively improved. Fig. 3(c) is the desired result in which both the resolution and contrast are significantly enhanced.

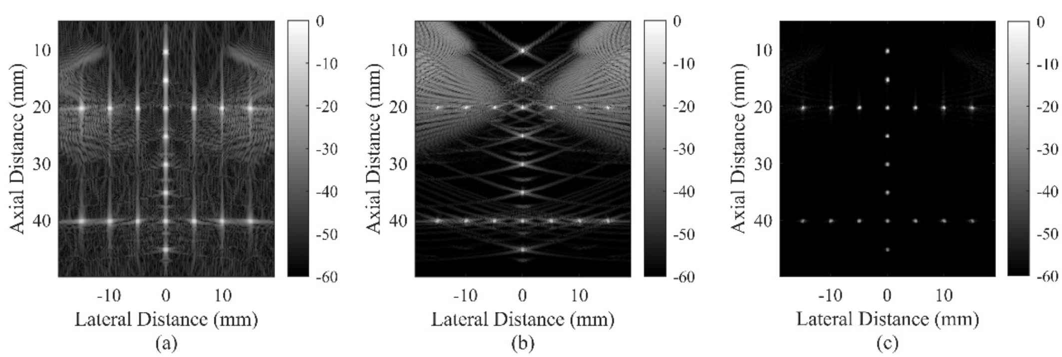

Figure 3: Images of simulated point targets acquired by beamforming methods: (a) FM-HFR, (b) DAS-HFR, (c) proposed method

The axial cross section across the point targets in the middle of the imaging area with x=0 along the axial direction (0, z), is given in Fig. 4. The sidelobe in an ultrasound image will significantly impact the effective dynamic range which can reflect the contrast improvement. Thus, the effective dynamic range, which is defined as the minimum peak mainlobe to the maximum peak sidelobe, was measured to illustrate the image quality. The image resolution is evaluated by the full width at half maximum (FWHM) which defined as the mainlobe beam width at -6 dB.

It can be seen that the effective dynamic ranges of the images reconstructed by FM-HFR algorithm and the DAS-HFR algorithm along the axial direction are about 16 dB and 17 dB, while the weighted imaging result is close to 25 dB. The dynamic range of the proposed image is significantly improved. Fig. 5 shows lateral distribution of the first row of scattering points at 20 mm depth. The effective dynamic ranges of the imaging results from FM-HFR and DAS-HFR are about 28 dB and 32 dB, while the weighted imaging results are about 43 dB. The axial effective dynamic range is lower than the lateral effective dynamic range for the case of the signal intensity falling with increasing depth caused by attenuation. Generally, the proposed method can increase the dynamic range of an image by nearly 10 dB. We calculated the average lateral FWHM to quantify the image resolution. FM-HFR and DAS-HFR achieve average lateral FWHMs of 0.54 mm and 0.35 mm, respectively, while the proposed method provides a better resolution performance with the average lateral FWHM of 0.30 mm.

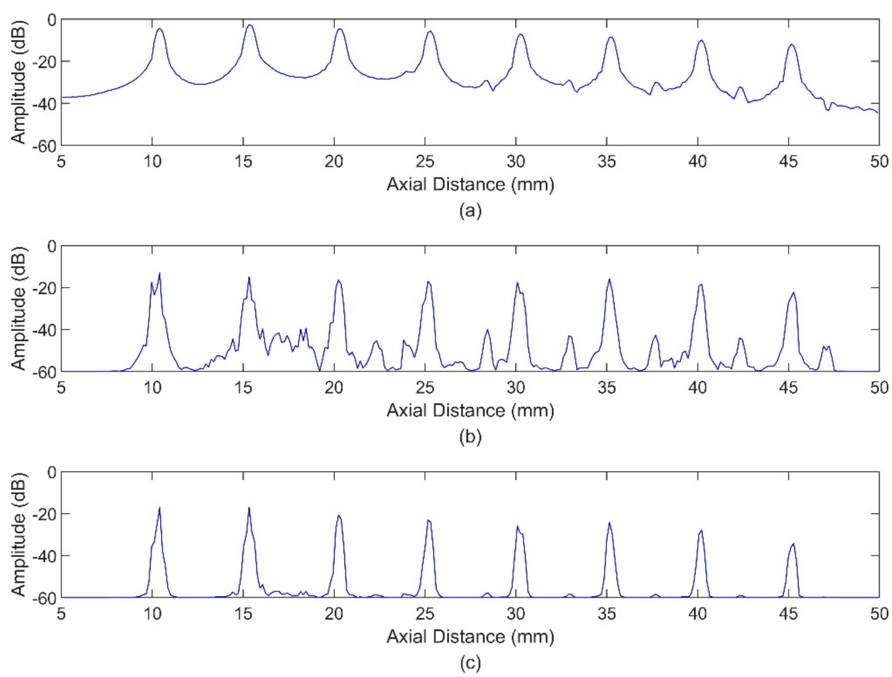

Figure 4: Axial cross section through the middle eight point targets along the axial direction in the simulated image of (a) FM-HFR, (b) DAS-HFR, (c) proposed method

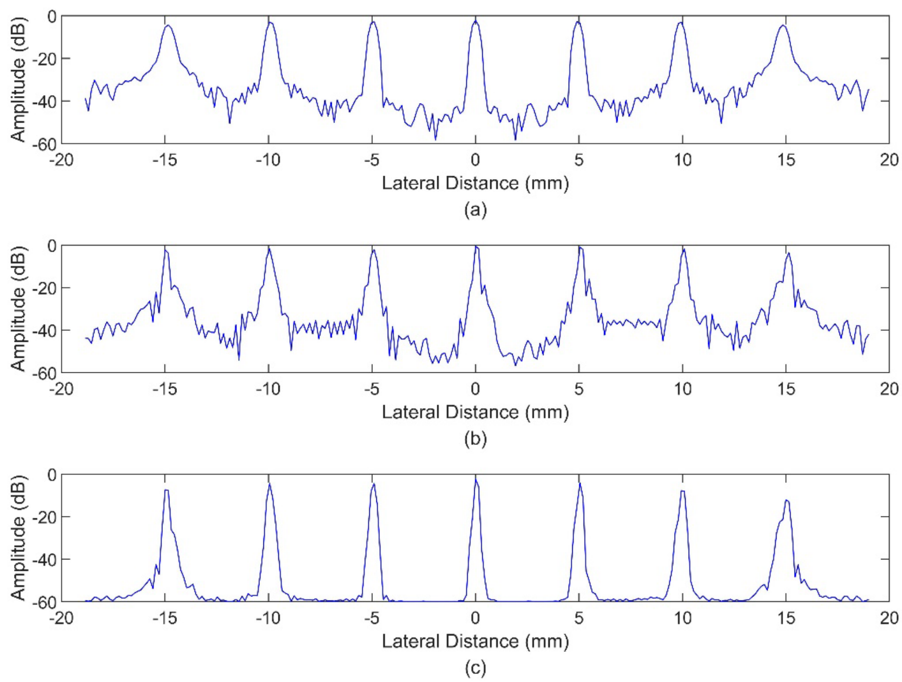

Figure 5: Lateral cross section through the seven point targets at 20 mm depth in the simulated image of (a) FM-HFR, (b) DAS-HFR, (c) proposed method

3.3 Experiment result

In the experimental data, the imaging target is a standard ultrasound phantom that consists of speckle-generating targets and several scattering points. The echo signal is collected by an open multi-channel ultrasound research platform (Vantage 256 scanner produced by Verasonic, United States).

Fig. 6 is the imaging results of the experimental phantom. The reconstructed images are shown with a dynamic range of 60 dB. Figs. 6(a) and 6(b) present the imaging results of the FM-HFR and the DAS-HFR, respectively. Fig. 6(c) shows the imaging result obtained by Eq. (14). From Figs. 6(a) and 6(b), the imaging quality of FM-HFR and DAS-HFR are similar. Specifically, the speckle is a little better in Fig. 6(a), but the axial resolution is not high. The axial resolution in Fig. 6(b) is better than in Fig. 6(a), but the lateral resolution is poor. In the shallow region of Fig. 6(b), two point targets are not visible and there are some artifacts on the left and right sides. Fig. 6(c) has the best resolution, and the contrast is also significantly improved.

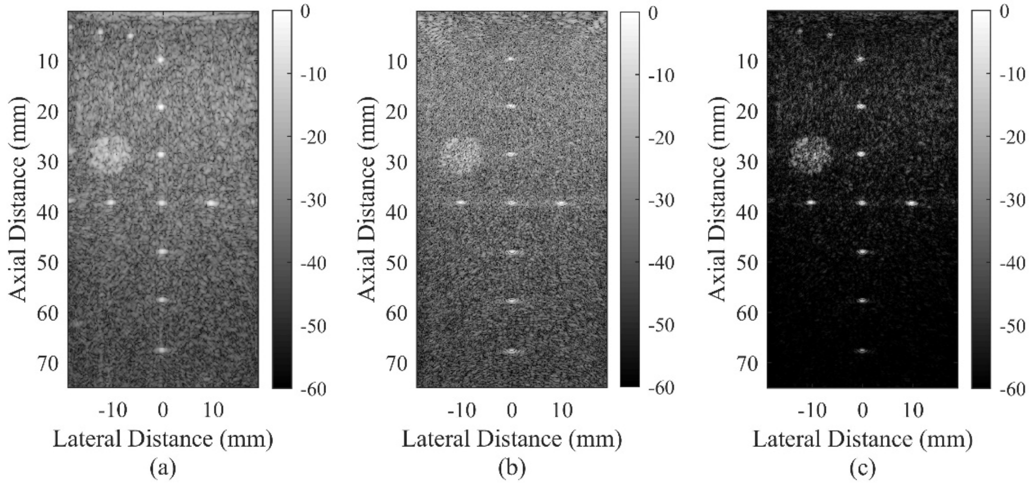

Figure 6: Images of experimental point targets acquired by different beamforming methods: (a) FM-HFR, (b) DAS-HFR, (c) proposed method

Fig. 7 gives the axial cross sections of the point targets located at x=0 mm, and The lateral cross sections for point targets at z=38 mm are shown in Fig. 8. The effective dynamic range of the imaging results from FM-HFR and DAS-HFR algorithm along the axial direction are found to be about 6 dB and 5 dB due to the noise interference and signal attenuation. For the proposed method, the dynamic range is about 14 dB. As shown in Fig. 8, FM-HFR and DAS-HFR have an effective dynamic range of about 18 dB and 11dB along lateral direction, while the effective dynamic range of the proposed method is about 28 dB. And the sidelobe is effectively suppressed. In experiment, the average lateral FWHMs of FM-HFR and DAS-HFR are 0.93 mm and 0.87 mm, while it is 0.56 mm for the proposed method. Therefore, the reconstructed image also has significantly improved resolution and contrast.

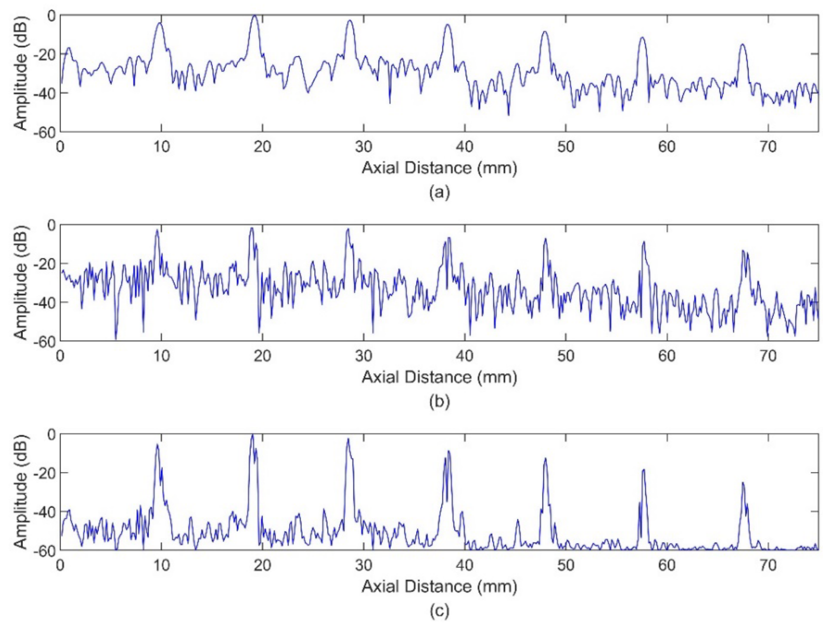

Figure 7: Axial cross section through the middle eight point targets along the axial direction in the experimental image of (a) FM-HFR, (b) DAS-HFR (c) proposed method

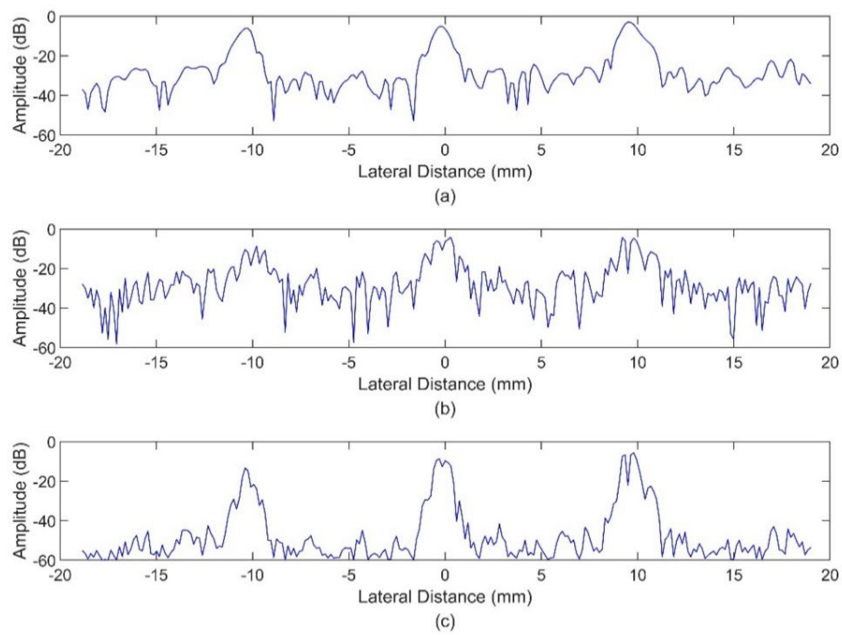

Figure 8: Lateral cross section through the three point targets at 38 mm depth in the simulated image of (a) FM-HFR, (b) DAS-HFR, (c) proposed method

4 Discussion

The proposed algorithm uses the imaging results of DAS-HFR to weight the imaging results of FM-HFR. These methods are consistent with using FM-HFR to weight the imaging results of DAS-HFR. The former expression is adopted due to the following considerations: The core of the FM-HFR algorithm is a Fourier transformation, which is known to be global in terms of time or space domain. That is to say, if no special processing is done, the FM-HFR algorithm directly generates an image of the whole imaging region. However, DAS-HFR imaging is carried out in the time domain, and it is possible to image the designated area of the imaging target by controlling the delay time τ_j. We can make use of the characteristics of FM-HFR imaging and DAS-HFR imaging. For example, when imaging the target, we first use the FM-HFR method to obtain the global image with a low imaging quality as shown in Figs. 9(a) and 10(a). Then, we observe the global image and find the imaging area of interest. Additionally, DAS-HFR is used to image this area of interest and obtain the constructed area image to weight the global image. Finally, we can obtain the whole area image, which includes the local image with high image quality as shown in Figs. 9(b) and 10(b). Therefore, the proposed method not only makes use of the efficiency of the FM-HFR algorithm, but also takes advantage of DAS-HFR local imaging.

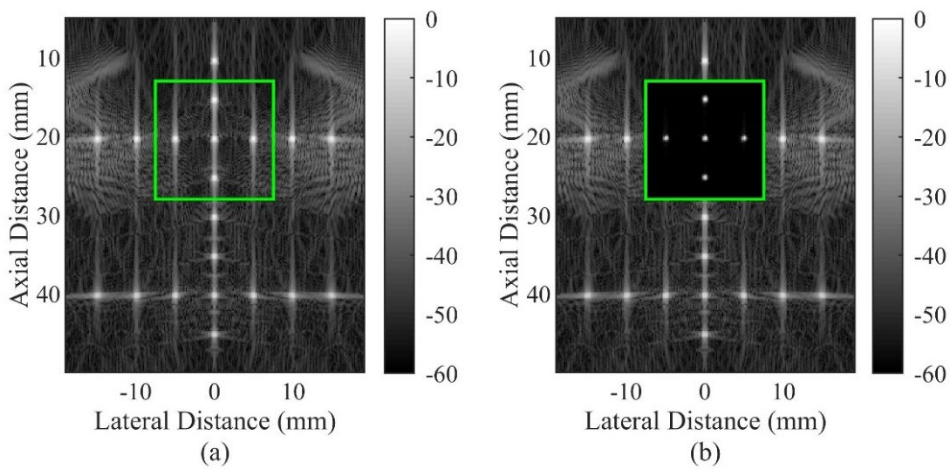

Figure 9: (a) Simulated point target images obtained with FM-HFR. (b) Simulated point target images including a local image with high image quality

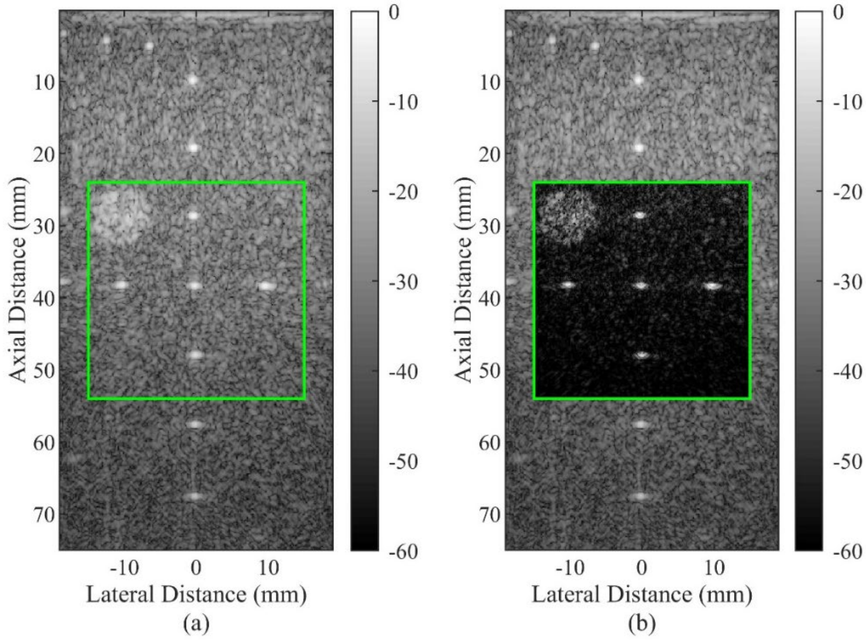

Figure 10: (a) Experimental point target images obtained with FM-HFR. (b) Experimental point target images including a local image with high image quality

We can also roughly quantify the delay time τ_j and obtain a rough DAS-HFR global imaging on the premise of reducing the computational load. Then, the result is used to weight the FM-HFR imaging to slightly improve the image quality. If the image has diagnostic value, we can further and precisely quantify the delay time τ_j. Then, a clearer image is gradually reconstructed using the DAS-HFR imaging results to weight the FM-HFR imaging results. Furthermore, multi-core processors can be utilized to implement parallel computing for the proposed method to increase computation speed. With a powerful computer, DAS-HFR and FM-HFR beamforming algorithms can be performed simultaneously to achieve general quality images, then a high quality image is obtained by the proposed method.

5 Conclusion

This paper proposes a joint DAS and Fourier beamforming method for HFR imaging based on a DAS and FM-HFR imaging algorithm, which is, in-turn, based on the angular spectrum propagation principle. Although both imaging systems can achieve 3700 imaging frame rates, the image quality is poor. For the image quality improvement of the HFR ultrasound imaging system, the proposed method combines the results of DAS-HFR imaging and FM-HFR imaging to make good use of the different characteristics of the sidelobes of DAS-HFR imaging and FM-HFR imaging, and adopts DAS-HFR imaging to weight FM-HFR imaging. The simulation and experimental results indicate the effectiveness of the joint DAS and Fourier beamforming method, which improves the effective dynamic range and resolution of HFR ultrasound images. Therefore, the proposed method is significance for research on HFR imaging.

Acknowledgement: This work is supported by National Natural Science Foundation of China (Project Nos. 61201060 and 61172037).

Funding Statement: This work is supported by National Natural Science Foundation of China, http://www.nsfc.gov.cn/. Peng H. received the project No. 61172037 and Zheng C. received the project No. 61201060.

Conflicts of Interest: The authors declare that they have no conflicts of interest to report regarding the present study.

References

Chau, G.; Lavarello, R.; Dahl, J. (2016): Short-lag spatial coherence weighted minimum variance beamformer. *IEEE International Ultrasonics Symposium*, pp. 1-3.

Chen, C.; Hendriks, G. A. G. M.; van Sloun, R. J. G.; Hansen, H. H. G.; de Korte, C. L. (2018): Improved plane-wave ultrasound beamforming by incorporating angular weighting and coherent compounding in fourier domain. *IEEE Transactions on Ultrasonics, Ferroelectrics, and Frequency Control*, vol. 65, pp. 749-765.

Cheng, J.; Lu, J. Y. (2006): Extended high-frame rate imaging method with limited-diffraction beams. *IEEE Transactions on Ultrasonics, Ferroelectrics, and Frequency Control*, vol. 53, pp. 880-899.

Diamantis, K.; Greenaway, A.; Anderson, T.; Jensen, J. A.; Sboros, V. (2017): Experimental performance assessmentof the sub-band minimum variance beamformer for ultrasound imaging. *Ultrasonics*, vol. 79, pp. 87-95.

Du, H.; Peng, H.; Jiang, Z.; Feng, H. (2007): Study on the property of the second harmonic in the nearfield of a Bessel ultrasonic field based on the Fourier-Bessel series. *Acta Physica Sinica*, vol. 56, pp. 6496-6502.

Han, Z.; Peng, H.; Zhao, X.; Chen, X. (2018): 3D ultrasound imaging in frequency domain based on concepts of array beam and synthetic aperture. *Ultrasonics*, vol. 84, pp. 254-263.

Jensen, J. A. (1996): Field: a program for simulating ultrasound systems. *Medical & Biological Engineering & Computing*, vol. 34, pp. 351-353.

Jensen, J. A.; Svendsen, N. B. (1992): Calculation of pressure fields from arbitrarily shaped, apodized, and excited ultrasound transducers. *IEEE Transactions on Ultrasonics, Ferroelectrics, and Frequency Control*, vol. 39, pp. 262-267.

Liebgott, H.; Rodriguez-Molares, A.; Cervenansky, F.; Jensen, J. A.; Bernard, O. (2016): Plane-wave imaging challenge in medical ultrasound. *IEEE International Ultrasonics Symposium*, pp. 1-4.

Lu, J. Y. (1997): 2D and 3D high frame rate imaging with limited diffraction beams. *IEEE Transactions on Ultrasonics, Ferroelectrics, and Frequency Control*, vol. 44, pp. 839-856.

Lu, J. Y.; Cheng, J. (2005): Field computation for two-dimensional array transducers with limited diffraction array beams. *Ultrasonic Imaging*, vol. 27, pp. 237-255.

Lu, J. Y.; Greenleaf, J. F. (1990): Ultrasonic nondiffracting transducer for medical imaging. *IEEE Transactions on Ultrasonics, Ferroelectrics, and Frequency Control*, vol. 37, pp. 438-447.

Peng, H.; Lu, J. Y.; Han, X. (2006): High frame rate ultrasonic imaging system based on the angular spectrum principle. *Ultrasonics*, vol. 44, pp. e97-e99.

Peng, J.; Peng, H. (2012): Chaotic frequency-modulating continuous wave for an ultrasonic doppler blood flow velocity measurement system. *Acta Physica Sinica*, vol. 61, pp. 248701.

Ranganathan, K.; Walker, W. F. (2003): A novel beamformer design method for medical ultrasound. Part Ⅰ: Theory. *IEEE Transactions on Ultrasonics, Ferroelectrics, and Frequency Control*, vol. 50, pp. 15-24.

Synnevag, J.; Austeng, A.; Holm, S. (2007): Adaptive beamforming applied to medical ultrasound imaging. *IEEE Transactions on Ultrasonics, Ferroelectrics, and Frequency Control*, vol. 54, pp. 1606-1613.

Synnevag, J.; Austeng, A.; Holm, S. (2009): Benefits of minimum-variance beamforming in medical ultrasound imaging. *IEEE Transactions on Ultrasonics, Ferroelectrics, and Frequency Control*, vol. 56, pp. 1868-1879.

Wang, Y.; Zheng, C.; Peng, H.; Chen, Q. (2018): An adaptive beamforming method for ultrasound imaging based on the mean-to-standard-deviation factor. *Ultrasonics*, vol. 90, pp.32-41.

Wei, Y. M.; Peng, H. (2014): Study on the transmission system of high frame rate ultrasonic imaging based on the non-diffraction wave. *Acta Physica Sinica*, vol. 63, pp. 198702.

Zhao, J.; Wang, Y.; Yu, J.; Guo, W.; Li, T. et al. (2016): Subarray coherence based postfilter for eigenspace based minimum variance beamformer in ultrasound plane-wave imaging. *Ultrasonics*, vol. 65, pp. 23-33.

Zheng, C.; Wang, H.; Xu, X.; Peng, H.; Chen, Q. (2020): An adaptive imaging method for ultrasound coherent plane-wave compounding based on the subarray zero-cross factor. *Ultrasonics*, vol. 100, pp. 105978.